Int J CARS (2016) 11:1821–1829
DOI 10.1007/s11548-015-1341-8

ORIGINAL ARTICLE

Robot-assisted automatic ultrasound calibration

Fereshteh Aalamifar[1] · Alexis Cheng[1] · Younsu Kim[1] · Xiao Hu[1] · Haichong K. Zhang[1] · Xiaoyu Guo[1] · Emad M. Boctor[1]

Received: 18 January 2015 / Accepted: 23 December 2015 / Published online: 11 January 2016

Abstract

Purpose Ultrasound (US) calibration is the process of determining the unknown transformation from a coordinate frame such as the robot's tooltip to the US image frame and is a necessary task for any robotic or tracked US system. US calibration requires submillimeter-range accuracy for most applications, but it is a time-consuming and repetitive task. We provide a new framework for automatic US calibration with robot assistance and without the need for temporal calibration.

Method US calibration based on active echo (AE) phantom was previously proposed, and its superiority over conventional cross-wire phantom-based calibration was shown. In this work, we use AE to guide the robotic arm motion through the process of data collection; we combine the capability of the AE point to localize itself in the frame of the US image with the automatic motion of the robotic arm to provide a framework for calibrating the arm to the US image automatically.

Results We demonstrated the efficacy of the automated method compared to the manual method through experiments. To highlight the necessity of frequent ultrasound calibration, it is demonstrated that the calibration precision changed from 1.67 to 3.20 mm if the data collection is not repeated after a dismounting/mounting of the probe holder. In a large data set experiment, similar reconstruction precision of automatic and manual data collection was observed, while the time was reduced by 58 %. In addition, we compared ten automatic calibrations with ten manual ones, each performed in 15 min, and showed that all the automatic ones could converge in the case of setting the initial matrix as identity, while this was not achieved by manual data sets. Given the same initial matrix, the repeatability of the automatic was [0.46, 0.34, 0.80, 0.47] versus [0.42, 0.51, 0.98, 1.15] mm in the manual case for the US image four corners.

Conclusions The submillimeter accuracy requirement of US calibration makes frequent data collections unavoidable. We proposed an automated calibration setup and showed feasibility by implementing it for a robot tooltip to US image calibration. The automated method showed a similar reconstruction precision as well as repeatability compared to the manual method, while the time consumed for data collection was reduced. The automatic method also reduces the burden of data collection for the user. Thus, the automated method can be a viable solution for applications that require frequent calibrations.

Keywords US calibration · Automatic calibration · Robotic US

✉ Fereshteh Aalamifar
fereshteh@jhu.edu

Alexis Cheng
acheng22@jhu.edu

Younsu Kim
ykim99@jhu.edu

Xiao Hu
xhu@jhu.edu

Haichong K. Zhang
hzhang61@jhu.edu

Xiaoyu Guo
xguo9@jhu.edu

Emad M. Boctor
eboctor1@jhmi.edu

[1] Johns Hopkins University, Baltimore, MD, USA

Introduction

Ultrasound (US) imaging has grown quickly recently due to its real-time, low-cost, and non-ionizing radiation properties. Many recent applications have integrated robotic arms or tracking systems to US imaging [1–7]. In such systems, US calibration is a necessary task to localize 3D position and orientation of the US image, or US transmitter/receivers in the robot tooltip, tracked marker, or other coordinate frames (called "moving frame," while the fixed frame, e.g., robot base or tracking system, is called "world's frame"). In most tracked or robotic US systems, very accurate (millimeter or submillimeter range) calibrations are required. However, millimeter-range errors can easily happen after the calibration due to unwanted bending/deformations, tightening/untightening screws, or even environmental changes. These types of accuracy degradation require the user to recalibrate frequently.

Several US calibration methods are commonly used in robotic or tracked US applications [8]. Some methods require building a calibration phantom [9–17], while others collect data from a point, a stylus, or the bottom of a water tank [18–22]. Every US calibration requires collecting data from US machine and another machine such as a tracker or a robot controller. US calibration methods, from the data collection point of view, can be categorized into two types: real-time data collection (also called freehand) and static data collection. A clear advantage of real-time data collection is that it easily collects a rich amount of data in a short period of time. However, in real-time data collection, the two machines should be temporally calibrated beforehand to determine the correspondence between data sets. Temporal calibration adds to the complexity of the calibration procedure and also can by itself be a source of error [9,10]. To avoid temporal calibration, the user can move the probe to the desired position but collect and label data when all the components are in a static position. This is called static data collection and is generally a time-consuming approach. In addition, in some applications, when a robotic arm is involved, it might be difficult for the user to operate the arm by hand to collect data in real time. For these reasons, in this paper, we focus on static methods. Among the static methods, one of the most commonly used is point calibration, in which a single point is imaged from different positions and orientations [8]. At each pose, the location of the point in the US image frame and also the location of the moving frame in the world's frame are recorded. Then, the rigid transformation between the moving frame and the US image frame is calculated. However, at each point, the user needs to make sure that the point is in the image mid-plane [10,22].

Guo et al. [22] previously proposed a static type of US calibration using an AE point and showed its superiority over single-point cross-wire calibration. The active echo element (AE) is a tiny US element capable of transmitting/receiving US signals. If used as a fixed point fiducial, the AE can evaluate the signal energy it receives from elements of the US probe and provide feedback on how close it is to the image mid-plane. In this work, we close the loop with the robotic arm controller and use the feedback from the AE to drive the robotic arm in order to align the AE fiducial with the US image mid-plane. In addition, since the AE can localize itself in the US image frame, using US time-of-flight information, fully automatic data collection using the robotic arm can be achieved. Furthermore, the robot can automatically pause at each pose for data collection; therefore, temporal calibration of the machines involved in the spatial US calibration is not necessary.

In summary, AE calibration does not need temporal calibration and is more accurate than cross-wire point-based calibration [22]. Additionally, its active communication with the US probe can guide a robotic arm for automatic data collection. In this paper, we provide the materials and methods for preparing the setup and for data processing and calculations. Then, the robot motion planning for data collection is explained. Next, we compare the results of manual and automatic data collection to validate the automated method through extensive experiments. It should be noted that in this paper, we refer to the use of the robot control panel by a human to collect data sets one by one as manual. It might be seen by some as a semiautomatic method because the user has the capability to control the arm using buttons and enjoy the stability of this type of control. This kind of data collection, even though still time-consuming and tiring, provides a high-quality data set, and we show that automating this process does not degrade the quality.

Materials and methods

In this section, we explain the materials and methods required for US calibration data collection and calculation. Finally, the algorithmic framework and developed software tools are described.

AE US element

In a point-based calibration, ensuring that the point fiducial is in the US image mid-plane is necessary to achieve an accurate calibration. Guo et al. [23] demonstrated an active US pattern injection system (AUSPIS), which solves the mid-plane error problem. AUSPIS has a miniaturized US element, AE, which senses the beacon pulse transmitted by an US probe. The AE element is made of a customized PZT5H tube with an outer diameter of 2.08 mm, an inner diameter of 1.47 mm, and a length of 2 mm. The electronic system includes a transmit/receive switch, an impedance matching circuit, a variable

gain amplifier, filters, a triggering circuit, an analog to digital converter, a microprocessor, and a pulser. The measured US signal intensity, by AE, will vary with distance from the US mid-plane, and hence, the maximum intensity can be used to ensure the AE element is in the US mid-plane. Guo et al. [22] also showed that the AE point could be used in the same way as a cross-wire point for the purposes of US calibration. The main advantages that the AE point has when compared to cross-wire points is that it can provide feedback to allow the AE element to be better positioned in the US mid-plane and that it can be automatically localized based on the received beacon pulses.

The AE circuitry can be connected to the PC using a USB cable; the signal intensity, and the location of the AE in the US image can be read from the serial port. The values provided by the AE system are:

- *ntotal*: total number of line triggers in one US frame (usually set to the number of elements in the US probe);
- *DLY*: the shortest time of flight (in samples) from US probe elements to the AE element;
- *ES*: the element number with the shortest *DLY;*
- *TC:* total number of counts for which the received signal is higher than the set threshold.

TC is used to determine how close the AE is to the image mid-plane; ideally, this variable should be maximized. To automatically localize the AE element position in the US image, the axial and lateral distances of the AE from the center element of the US probe are calculated. When using a linear US probe, axial and lateral distances can be found using the following equations:

$$x = L_{\text{probe}} \frac{(ES - (0.5\,\text{ntotal} + 0.5)}{\text{ntotal}}, \tag{1}$$

$$z = 1000\,\text{DLY} \cdot f \cdot \text{SOS}, \tag{2}$$

where L_{probe} is the US probe's length, f is the AE receiver sampling frequency, SOS is the speed of sound in the medium between the probe and AE, and $(x, 0, z)$ is the location of the AE in US image frame in millimeters (when defining the image origin at the center top of the image, as shown in Fig. 1). The reason for having the coefficients 0.5 in Eq. (1) is to set the image frame origin at the center top of the image, i.e., center of the center element of the probe.

Calibration calculations

In a point-based US calibration, a fiducial point is fixed in the world frame and then imaged by the US probe from various positions and orientations. For calibrating the robot tooltip to US image coordinate system, we considered the robot base frame as the world frame, then fixed the AE element inside a water tank. In a manual data collection, the robotic arm, holding the US probe, is moved to different positions and orientations. At each position, the US image mid-plane needs to be aligned with the AE element. Then, the arm is fixed, and the robot tooltip positions and orientation in the robot base, as well as the position of the AE in US image, are stored. Because data are collected when everything is at a static position, no temporal calibration between the US machine and robot controller is needed. Since the AE is fixed in the robot base frame, assuming no noise or measurement inaccuracy, the following holds:

$$B_i X p_i = P, \quad \forall i \tag{3}$$

where B_i is the 4×4 transformation matrix from robot base to its tooltip; X is the desired 4×4 calibration matrix, i.e., the transformation matrix from robot tooltip to US image frame; p_i is the homogenous representation of the AE element position in the US image frame; P is the homogenous representation of the AE element position in the robot base frame. Therefore, for any pairs of i and j, we have:

$$B_i X p_i = B_j X p_j, \quad \forall i, j \tag{4}$$

The above equation can be solved for X in an iterative manner. We used the gradient descent algorithm [24] to calculate the calibration matrix.

Automatic calibration framework

Since the AE can communicate with the US probe attached to the robotic arm, the whole process of robot movement and alignment with the AE element can be programmed into the robot controller. This way, the user will be able to do the US calibration with the press of a button. In this section, we provide the automatic calibration setup, robot motion definition, and the software module.

Automatic calibration setup

Figure 1 shows the necessary components of the automatic calibration setup. We used an Ultrasonix Sonixtouch machine, 4 cm, 128 arrays linear Ultrasonix probe (Analogic US, Richmond, BC, Canada), and the UR5 6° of freedom robotic arm (Universal robots, Odense, Denmark). UR5 is a compact light-weight robot with 85-cm spherical reach and 0.1-mm repeatability. Its tooltip is 7.5 cm in diameter. Together with the other characteristics, this arm is a suitable option for operating an US probe. A holder was designed and 3D printed to rigidly attach the probe to the robot tooltip.

The AE is synchronized with US probe using the trigger out of the US machine and sends data through the serial port. The US machine with the research license has a Windows XP

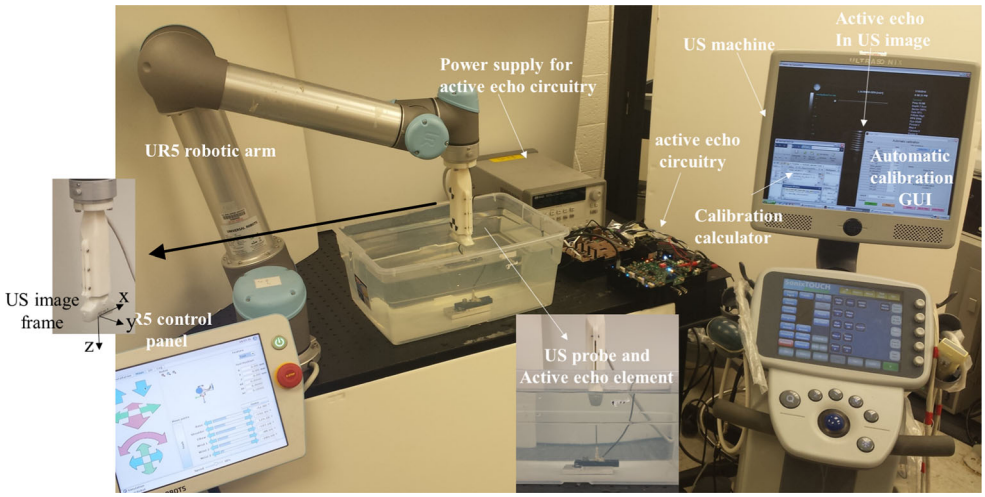

Fig. 1 Automatic calibration setup. The setup consists of a robotic arm, an US machine and probe, and the AE element with its driving circuits. The US image frame is shown on the *left*

Fig. 2 Different modules of automatic calibration setup and the way they communicate

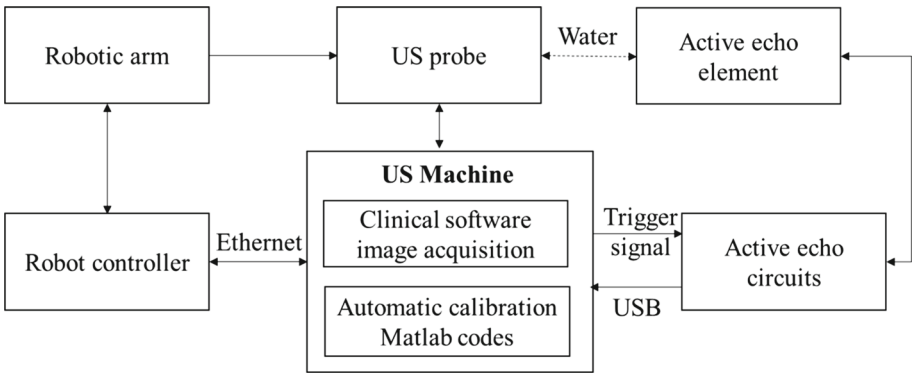

operating system that can be used to run the MATLAB software tool we prepared for the automatic calibration (will be explained in next section). This software controls the robotic arm by sending commands to the robot controller via Ethernet connection. Figure 2 shows different modules of the system setup.

Robot motion's definition

Robot motion was defined based on an initial estimation of the X matrix. The rotation part is estimated by asking the user to move the tooltip along axes of the US image, while the translation part is determined by measurements. It should be noted that the accuracy of the estimated X only affects the robot motion and not the accuracy of collected data or calibration results.

The robot workspace was considered as the area available above the water tank. First, the user determines three points of the workspace that initialize the motion definitions:

1. Origin (O): The user is requested to move the robotic arm such that the US probe is looking down on one side of the AE (with its center in line with the AE point), and the US image is almost perpendicular to the bottom of the water tank. This will be the starting point of the robot motion.
2. X axis point (P_x): The user is requested to move the robotic arm such that the US probe translates along its lateral.
3. Y axis point (P_y): The user is requested to move the robotic arm such that the probe translates from origin to a point along the elevational axis of the probe.

An example set of the above three points is shown in Fig. 3a. It should be noted that it is enough to define these points roughly as described. These points define the rotation part of the initial X matrix.

The robot tooltip's starting position is at point O. The rest of the robot motion/positions is defined as shown in Fig. 3b as follows:

1. The robot moves the probe in small defined steps (e.g., 2 mm) along the Y axis of the image and, at each step, checks the TC from AE. When TC decreases, it moves

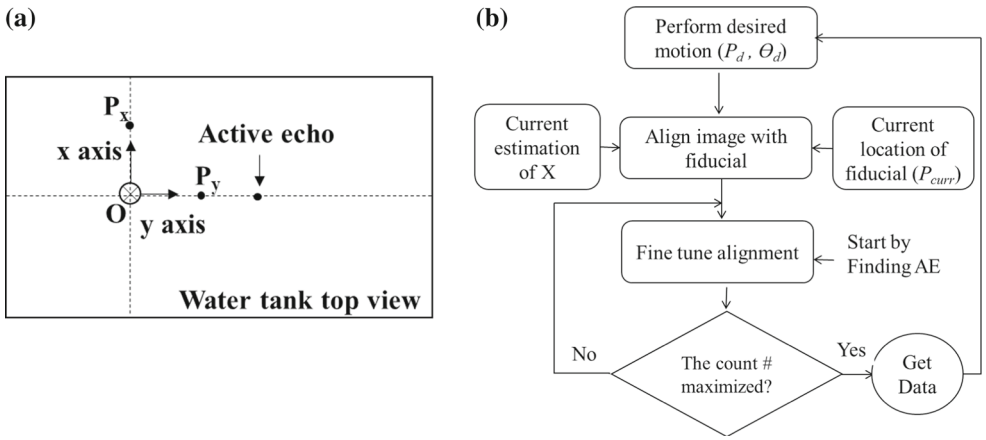

Fig. 3 **a** The initial points defined by the user to determine the virtual coordinate frame. The figure shows the water tank's *top* view. **b** Data collection workflow

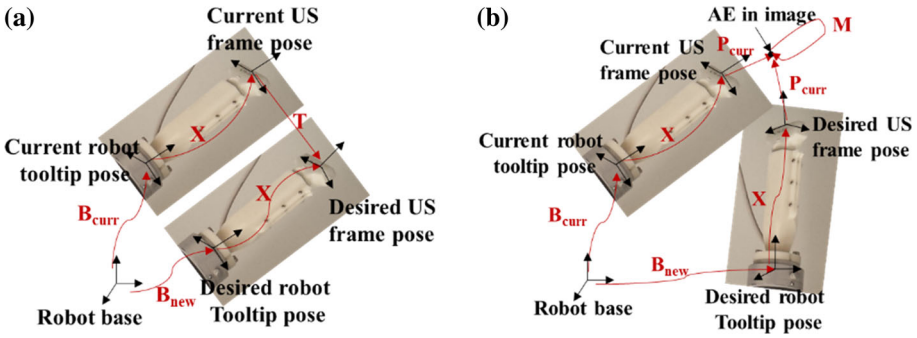

Fig. 4 **a** Transformations involved in calculating robot motion for aligning AE with image mid-plane as described in Eq. (5); T is a translation along Y axis of the image **b** remote center motion of the US image around the AE as described in Eq. (6)

the probe back by twice the step size and starts the search using a smaller step. As shown in Fig. 4a, to perform this motion, a sequence of robot poses should be calculated using the following equation:

$$B_{\text{new}} = B_{\text{curr}} X T X^{-1}, \tag{5}$$

where B_{new} and B_{curr} are new and current robot poses, respectively; X is the estimated calibration matrix; T is defined as:

$$T = \begin{bmatrix} & 0 \\ I_{3\times3} & \text{step} \\ & 0 \\ 0_{1\times3} & 1 \end{bmatrix}.$$

2. After several iterations, the robot moves with 0.1-mm steps and stores several (e.g., 6) TC values around the AE; it then moves the probe to the pose with maximum TC; hence, AE is aligned with image mid-plane with 0.1-mm accuracy now.
3. The program stores this point as the new origin, then collects the robot tooltip pose in the robot base frame and the AE pose in the US image as one data set.
4. The robot rotates around AE and at each rotation moves the probe s.t. the AE appears at different location in the image. The amounts of rotation and AE locations are defined by the user, as if the user would rotate or translate the probe by those amounts in a manual data collection. The robot pose for the rotations, as shown in Fig. 4b, can be defined as:

$$B_{\text{new}} = B_{\text{curr}} X T M T^{-1} X^{-1}, \tag{6}$$

where

$$M = \begin{bmatrix} e^{\begin{bmatrix} 0 & -\theta_z & \theta_y \\ \theta_z & 0 & -\theta_x \\ -\theta_y & \theta_x & 0 \end{bmatrix}} & \begin{matrix} 0_{3\times1} \\ 1 \end{matrix} \\ 0_{1\times3} & \end{bmatrix},$$

$$\text{and } T = \begin{bmatrix} I_{3\times3} & P_{\text{curr}} \\ 0_{1\times3} & 1 \end{bmatrix}.$$

$\theta_d = (\theta_x, \theta_y, \theta_z)$ is the desired rotation about the three axes of the image in radian, and P_{curr} is the current location of AE in US image. The new robot pose for translations is calculated using Eq. (5) with T defined as:

$$T = \begin{bmatrix} I_{3\times3} & P_d - P_{\text{curr}} \\ 0_{1\times3} & 1 \end{bmatrix},$$

where P_d is the desired location of AE in US image.

5. After each rotation/translation, the robot moves the probe with amount, $adjust\_gap = -5$ mm, along image's Y-axis, then performs the AE alignment process until achieving 0.1-mm accuracy. Then, it records the data and moves to the next pose. Moving back the US probe along Y-axis ensures that AE is not located behind the US probe searching path due to inaccuracies, and the selected value for *adjust_gap* depends on the accuracy of estimated X.

While defining the robot motions, several safety considerations should be incorporated into the program. In our implementations, we added the safety considerations below. If the robot cannot find the AE within a set distance (e.g., 4 cm), it pauses and asks the user to adjust the AE sensitivity because, especially at large angles, the TC value stays 0 and the AE cannot be detected. This issue can be resolved in future versions by increasing the sensitivity and stability of AE measurements. Another safety consideration is to prevent the probe from touching the AE, because the program only determines the goal position of the robot tooltip, and the robot controller calculates the path to the goal positions; there might be a case where the path intersects the active echo location, and hence, the probe might hit the active echo during the move. To prevent this, we command the robot to go to a safe point (higher than the desired point) and then linearly move to the desired point.

Software module

We programmed the above-described robot motion, data collection, and processing as a MATLAB GUI, as shown in Fig. 5, that can be run on the US machine. Another MATLAB instance can run another module to calculate calibration from the collected data and show the current results in real time. This online calculation can also be used to update the X matrix estimation for robot motions. Once the user sets the parameters and can test the connections successfully, he/she can press the "Start" button to start the automatic calibration.

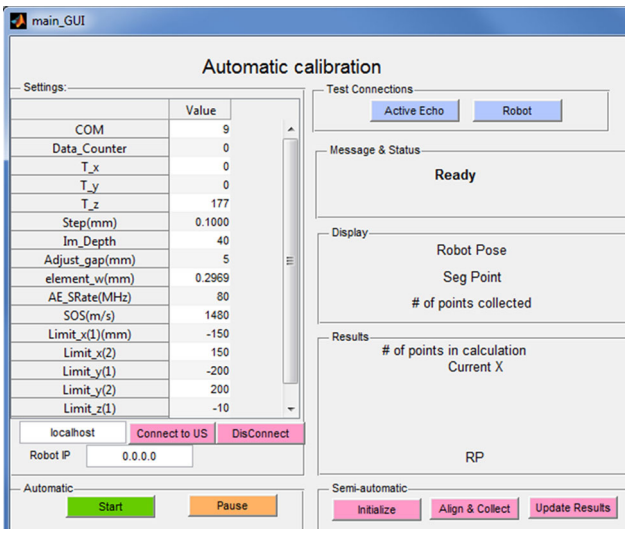

Fig. 5 MATLAB GUI

Experiments and results

Superiority of AE over cross-wire calibration was shown in [22]. In this section, the goal is to validate the automated AE framework. Several experiments were designed to evaluate the automated system. Even though AE automatic localization was used for robot motion planning, in all the experiments, the data were processed offline using manual segmentation of the B-mode image due to low receiving sensitivity of the available AE element.

Experiment I: effect of mounting/dismounting of US probe on calibration

In this experiment, we tried to quantify the effect of a mechanical change, as an example dismounting/mounting the probe holder, on the calibration matrix. In a case study, for an experiment that needed to be done with the robotic arm mounted on a cart, the probe was calibrated to the robot tooltip. Then, the robotic arm needed to be moved to another robot stand. For this reason, the probe holder had to be dismounted from the tooltip and mounted back after moving the robot. The same calibration procedure was repeated after re-attachment of the probe holder.

The probe is designed to be mounted only in one way, and the user tried to tighten the screws similar to the previous case. For each of the calibrations, 50 points were used for computing the calibration matrix, and 20 points to calculate the reconstruction precision (RP). The reconstruction precision is defined as the standard deviation of the evaluation points reconstructed in robot base using the computed calibration matrix. Table 1 shows the results. Case 1 relates to the data set collected before moving the robot, and case 2 relates to after movement. It is evident that, for both cases, the calibration data points were a better fit for the evaluation points collected in the same case. This experiment reveals the importance of repeating the calibration after a mechanical change.

Table 1 Comparison of reconstruction precision when repeating the calibration after a dismount/mount back of the probe from the tooltip

Calculation/evaluation	Case1/case1	Case1/case2	Case2/case2	Case2/case1
Norm (RP)	2.08	2.39	1.67	3.2

Experiment II: comparison of automatic versus manual without time constraint

In this evaluation, the calibration quality of the automated method was compared to that of the manual method; each data set contained 40 points. Additionally, 80 data points from a wide range of angles were collected for evaluation, to make sure the evaluation data set contained enough data, 40 by trained user, and 40 automatically. For a fair comparison, a trained user acquired data as the manual method. As a result, the norm reconstruction precisions for both data sets were 0.95 and 1.06 mm for manual and automatic methods, respectively. The reconstruction precisions were similar, though slightly lower for the automatic method, possibly because the user was given unlimited time to collect data, and therefore, more rotations were performed. The time spent to collect data was around 60 and 35 min for manual and automatic methods, respectively.

Experiment III: comparison of automatic versus manual with time constraint

In this experiment, the goal was to compare the calibration results when the same amount of time was spent by the user and the robot to collect data. In this experiment, the goal was to collect the most efficient data set in a short period of time. For the automatic method, this data set contained rotations of 30° and −30° about all the three axes, two translations for each rotation, and 2 extra points at 0 rotation, yielding collection of 14 data points in about 12 min. The user was also asked to collect as many data as possible in all axes in 15 min. The experiment was repeated ten times to produce statistically reliable results. The 80 evaluation data points from Experiment II were used to calculate RP.

Figure 6 shows the RP results, while Table 2 shows the comparison of repeatability. The repeatability is defined as the norm standard deviation of four corners of the image reconstructed in the robot tooltip using all computed X's. The four corners were considered as:

$$A = [-19, 0, 0],\ B = [19, 0, 0],\ C = [-19, 0, 40],\ D = [19, 0, 40]$$

In this experiment, the manual segmentation, and the initial value used for the gradient descent algorithm, $X0$, became more important due to the small available data sets for calibration. While all the automatically collected data sets converged when identity matrix was used as initial guess for gradient descent, only a few of the manual ones could converge. Hence, we tried an initial matrix close to the calibration matrix called $X1$. It is evident that, when using an initial matrix close to the solution, the manual data set could work similarly to the automatic one. However, the repeatability of the calculated X in manual case is larger than that achieved by the automatic data set.

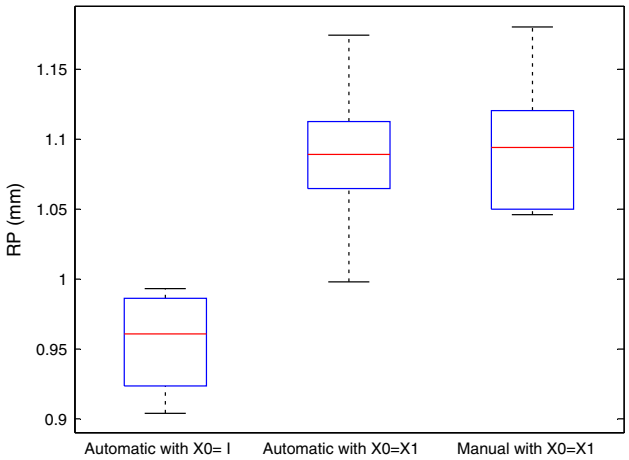

Fig. 6 Comparison of distribution of norm (RP) for ten times repeating data collection. The *red line* shows the median, the *blue box* edges show 25th and 75th percentiles, and the *black lines* show extreme values

Table 2 Comparison of repeatability for ten sets of manually and automatically collected data

	Repeatability (mm)
Automatic $X_0 = I$	[1.11, 1.14, 0.99, 0.52]
Automatic $X_0 = X1$	[0.46, 0.34, 0.80, 0.47]
Manual $X_0 = X1$	[0.42, 0.51, 0.98, 1.15]

Best repeatability was achieved with automatic data set using $X1$ as initial guess for gradient descent

Discussions

The experimental results show that the automated method provides similar repeatability and reconstruction precision to manual (or semiautomatic) data collection. Hence, automation does not affect the performance but provides easier and faster data collection. For applications where a massive number of calibrations are required, or when US calibration needs to be repeated frequently due to environmental, mechanical, or other changes, automatic framework can be a viable solution.

On the other hand, when automatic data collection is not possible, the manual data collection can be equivalently appropriate if (1) the calibration procedure is not frequent; (2) data are collected by a sufficiently representative number of points by performing enough rotations about the point fiducial; (3) data processing is done by trying various initial matrices in the case of a small data set for calibration.

The results of Experiment III reveal the importance of initial matrix selection for the gradient descent method. Hence, especially, for small data sets, it is recommended to try many

different initial matrices. Even for the automatic case, it is still important to try various initial matrices, since as shown by Fig. 6 and Table 2, better RP was achieved by setting $X_0 = I$ while it produced less repeatability. We surmise the reason is that, when the initial guess is farther from the solution, the gradient descent tries more variant X's and hence can find a better RP, while when choosing an X close to the solution, this is not the case.

The results of the automated framework lacks robust AE readings due to lower receiving sensitivity of the available AE US element in the setup, which requires setting the AE sensitivity at its control boards to maximum. This can be solved by changing the AE US element and its embedding design or by enabling control of sensitivity by the automatic program; i.e., at large angles, the sensitivity can be increased, while at small angles it is decreased. In addition, the AE can be designed to be embedded on a flat surface (rather than the tip of a needle), which provides more dexterity around the AE point, and safer robot motions, thus avoiding collision with the AE element. These improvements could potentially reduce the automatic data collection time almost by half and will also enable use of automatic segmentation for highly accurate calibrations.

In this paper, the robotic arm tooltip is the "moving frame." However, with some modifications, this method can be used to automate the calibration procedure in any application requiring accurate US calibration, for example when a tracked marker is the "moving frame," while the robot is used as an assistive arm to collect data. In addition, since submillimeter precision is usually desired for US calibrations, this procedure can be repeated regularly as a quick automatic improvement/update of the previously computed transformation matrix.

Finally, having an automated setup brings up an interesting question: What is the optimal robot maneuver for data collection? In other words, how much data, and in which poses with respect to the point fiducial, are necessary and sufficient to achieve the most accurate calibration possible? An interesting future step for the automated framework is to collect a large set of data at known angles and positions and devise an optimized and standardized calibration procedure.

Conclusions and future work

US calibration is required in most tracked or robot-assisted US systems, and it is time-consuming. On the other hand, the quality of the US calibration has a high impact on overall system functionality. Thus, repetition of data collection for calibration is unavoidable in many applications. In this paper, we proposed a robot-assisted framework to automatically perform an AE US calibration with high precision, minimal user dependency, and no need for temporal calibration.

We showed the preliminary design and experimental results to evaluate the efficacy of automatic calibration for a robot US calibration. However, the idea can be adapted for various applications requiring accurate US calibrations. This setup can also be used to investigate a standard optimized procedure for data collection. Hence, the same framework can be further developed to enable bootstrapping between the collected data and the quality of calibrations. For example, the program can perform an error analysis to determine where the database lacks enough data and command the robot to collect more data at those locations.

Acknowledgments We would like to thank Dr. Lei Chen for his valuable feedback on the accuracy of calibrated probe in various experiments and Dr. Xiaoyu Guo for providing the AE circuitry. Financial support was provided by Johns Hopkins University internal funds and NSF Grant IIS-1162095.

Compliance with ethical standards

Conflict of interest Authors have no conflict of interest with the content of this manuscript.

References

1. Ungi T, Lasso A, Fichtinger G (2015) Tracked US in navigated spine interventions. In: Li S, Yao J (eds) Spinal imaging and image analysis. Springer International Publishing, pp 469–494
2. Westwood JD (2014) An US-based navigation system for minimally invasive neck surgery. Med Meets Virtual Real 21 NextMed/MMVR21 196:36
3. Monfaredi R, Wilson E, Azizi koutenaei B, Labrecque B, Leroy K, Goldie J, Louis E, Swerdlow D, Cleary K (2014) Robot-assisted US imaging: overview and development of a parallel telerobotic system. Minim Invasive Ther Allied Technol 1–9
4. Sauer F, Khamene A, Bascle B, Schinunang L, Wenzel F, Vogt S (2001) Augmented reality visualization of ultrasound images: system description, calibration, and features. In Augmented reality, 2001. Proceedings IEEE and ACM international symposium on, pp 30–39. IEEE
5. Mebarki R, Krupa A, Chaumette F (2010) 2-d US probe complete guidance by visual servoing using image moments. Robot IEEE Trans 26(2):296–306
6. Chen TK, Leung C, Azar RZ, Chan K-K, Zhuang B, Dickie K, Dixon J, Pendziwol L, Pelissier L (2012) Laurent importance of transducer position tracking for automated breast US: initial assessments. In: Ultrasonics symposium (IUS), 2012 IEEE International. IEEE
7. Aalamifar F, Jiang D, Zhang HK, Cheng A, Guo X, Khurana R, Iordachita I, Boctor EM (2015) Co-robotic US tomography: dual arm setup and error analysis. In: Bosch JG, Duric N (eds) SPIE medical imaging. International Society for Optics and Photonics, Bellingham, p 94190N
8. Mercier L, Langø T, Lindseth F, Collins LD (2005) A review of calibration techniques for freehand 3-D US systems. US Med biol 31(2):143–165
9. Boctor EM, Iordachita I, Choti MA, Hager G, Fichtinger G (2006) Bootstrapped ultrasound calibration. Stud Health Technol Inform 119:61–66

10. Chen TK, Thurston AD, Ellis RE, Abolmaesumi P (2009) A real-time freehand ultrasound calibration system with automatic accuracy feedback and control. Ultrasound Med Biol 35(1):79–93
11. Chen TK, Thurston AD, Moghari MH, Ellis RE, Abolmaesumi P (2008) A real-time ultrasound calibration system with automatic accuracy control and incorporation of ultrasound section thickness. In: Miga MI, Cleary KR (eds) Medical imaging. International Society for Optics and Photonics, Bellingham, p 69182A
12. Boctor E, Viswanathan A, Choti M, Taylor RH, Fichtinger G, Hager G (2004) A novel closed form solution for ultrasound calibration. In: Biomedical imaging: nano to macro, 2004. IEEE international symposium on, pp. 527–530. IEEE
13. Viswanathan A, Boctor EM, Taylor RH, Hager G, Fichtinger G (2004) Immediate ultrasound calibration with three poses and minimal image processing. In: Barillot C, Haynor DR, Hellier P (eds) Medical image computing and computer-assisted intervention-MICCAI 2004. Springer, Berlin, pp 446–454
14. Dandekar S, Li Y, Molloy J, Hossack J (2005) A phantom with reduced complexity for spatial 3-D ultrasound calibration. Ultrasound Med Biol 31(8):1083–1093
15. Cheng A, Ackerman MK, Chirikjian GS, Boctor EM (2014) Design and development of an US calibration phantom and system. In: Yaniv ZR, Holmes DR (eds) SPIE medical imaging. International Society for Optics and Photonics, Bellingham, p 903624A
16. Hsu P-W, Prager RW, Gee AH, Treece GM (2008) Real-time freehand 3D US calibration. US Med Biol 34(2):239–251
17. Carbajal G, Lasso A, Gómez Á, Fichtinger G (2013) Improving N-wire phantom-based freehand US calibration. Int J Comput Assist Radiol Surg 8(6):1063–1072
18. Hsu P-W, Treece GM, Prager RW, Houghton NE, Gee Andrew H (2008) Comparison of freehand 3-D US calibration techniques using a stylus. US Med Biol 34(10):1610–1621
19. Melvær EL, Mørken K, Samset E (2012) A motion constrained cross-wire phantom for tracked 2D ultrasound calibration. Int J Comput Assist Radiol Surg 7(4):611–620
20. Zhang H, Banovac F, White A, Cleary K (2006) Freehand 3D ultrasound calibration using an electromagnetically tracked needle. In: Cleary KR, Galloway RL Jr (eds) Medical imaging. International Society for Optics and Photonics, Bellingham, p 61412M
21. Prager RW, Rohling RN, Gee AH, Berman L (1998) Rapid calibration for 3-D freehand US. US Med Biol 24(6):855–869
22. Guo X, Cheng A, Zhang HK, Kang H-J, Etienne-Cummings R,Boctor EM (2014) Active echo: a new paradigm for US calibration. In: Golland P, Hata N, Barillot C, Hornegger J, Howe R (eds) Medical image computing and computer assisted intervention-MICCAI 2014. Springer International Publishing, pp 397–404
23. Guo X, Kang H-J, Etienne-Cummings R, Boctor EM (2014) Active US Pattern Injection System (AUSPIS) for interventional tool guidance. PLoS One 9(10):e104262
24. Ackerman MK, Cheng A, Boctor E, Chirikjian G (2014) Online US sensor calibration using gradient descent on the Euclidean group. In: Robotics and automation (ICRA), 2014 IEEE international conference on. IEEE